

# Fano Resonance in a Quantum Wire with a Side-coupled Quantum Dot

Kensuke Kobayashi, Hisashi Aikawa, Akira Sano, Shingo Katsumoto, and Yasuhiro Iye  
*Institute for Solid State Physics, University of Tokyo, 5-1-5 Kashiwanoha, Chiba 277-8581, Japan*  
(Dated: February 8, 2020)

We report a transport experiment on the Fano effect in a quantum connecting wire (QW) with a side-coupled quantum dot (QD). The Fano resonance occurs between the QD and the “T-shaped” junction in the wire, and the transport detects anti-resonance or forward scattered part of the wavefunction. While in this geometry it is more difficult to tune the shape of the resonance than in the previously reported Aharonov-Bohm-type interferometer, the resonance purely consists of the coherent part of transport. By utilizing this advantage, we have qualitatively explained the temperature dependence of the Fano effect by including the thermal broadening and the decoherence. We have also proven that this geometry can be a useful interferometer to measure the phase evolution of electrons at a QD.

PACS numbers: PACS numbers: 73.21.La, 85.35.-p, 73.23.Hk, 72.15.Qm

## I. INTRODUCTION

The first observation of coherent transport in a mesoscopic system<sup>1</sup> opened up the field of electron interferometry in solids. Following that Aharonov-Bohm (AB) type interferometer, there appeared various types of electron interferometers including Fabry-Pérot type<sup>2</sup> and Mach-Zehnder type<sup>3</sup>. Such interferometry is of particular interest when the propagating electron experiences electronic states in a quantum dot (QD), because the interference pattern provides information on the physical properties such as electron correlation inside the QD. Several interferometry experiments have been reported for systems of a QD embedded in an AB ring<sup>4,5,6,7,8,9</sup>.

In these experiments one should keep in mind that the unitarity of electron wave propagation inevitably affects the transport property of the system. In the case of two terminal devices, for example, this results in the phase lapse of AB oscillation at the resonance<sup>10</sup>. While the resonance has such a subtle aspect, it brings interesting effects on the transport when it is positively used. A representative is the Fano effect<sup>11</sup>, which appears as a result of resonance between the localized state and the continuum. Although the Fano effect has been established in spectroscopy<sup>12</sup>, its general importance in mesoscopic transport is recognized only recently<sup>13,14</sup>. It has been predicted that the Fano effect appears in a QD embedded in an AB ring as schematically shown in Fig. 1 (a)<sup>15</sup>, and recently we have reported the experimental observation<sup>16,17</sup>.

The AB geometry has an advantage that the interference pattern can be tuned by the magnetic flux piercing the ring, while its spatial size tends to be large. In order to maintain the quantum coherence and to observe clearer effects, a smaller scale interferometer would be desirable. A candidate is a quantum wire (QW) with a finite length. A QD plus a connecting QW with measurement leads can be realized in the system schematically shown in Fig. 1 (b). Here the very short QW connecting the QD and the lead works as a resonator. We call this geometry a “side-coupled” QD or a “T-coupled” QD.

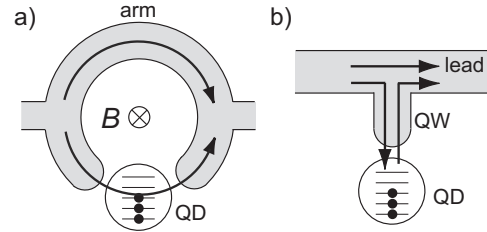


FIG. 1: (a) Schematic view of a Fano system consists of a QD and an AB ring. (b) Another type of Fano system consisting of a connecting quantum wire (QW) with a “T-coupled” quantum dot (QD).

The essential difference between this T-type Fano system and the QD-AB-ring system studied earlier lies in the fact that the interference detects the transmitted electrons in the latter case and the reflected electrons in the former case. Hence we can distinguish these two types of Fano effect as “reflection mode” and as “transmission mode”. While the Fano effect in the reflection mode has been discussed theoretically<sup>18,19,20,21,22,23,24</sup>, the experimental realization has been lacking.

In this Article, we report the first experimental observation of the Fano effect in a T-coupled QD. After briefing the experimental setup in Sec. II, evidence for the emergence of the Fano state in lowering the temperature is given in Sec. III A. We discuss the temperature dependence of the coherence measured in this geometry in Sec. III B. Then in Sec. III C, we show that the Fano effect in a T-coupled QD can be used to detect the phase shift in the scattering by the QD, which makes it a unique tool to investigate the phase and coherence of electrons in a QD.

## II. EXPERIMENT

To realize a T-coupled QD, we prepared the device shown in a scanning electron micrograph of Fig. 2. It

was fabricated from an AlGaAs/GaAs heterostructure by wet-etching. The characteristic of the two-dimensional electron gas (2DEG) were mobility =  $9 \times 10^5 \text{ cm}^2/\text{Vs}$ , sheet carrier density =  $3.8 \times 10^{11} \text{ cm}^{-2}$ , and electron mean free path  $l_e = 8 \mu\text{m}$ . This device is similar to what we previously studied<sup>16,17</sup>. Two sets of three fingers are Au/Ti metallic gates to control the local electrostatic potential. The three gates ( $V_R$ ,  $V_L$ , and  $V_g$ ) on the lower arm are used for defining and controlling the parameters of the QD with geometrical area of  $0.2 \times 0.2 \mu\text{m}^2$ .

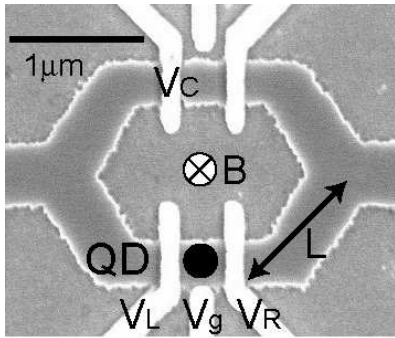


FIG. 2: Scanning electron micrograph of the device fabricated by wet-etching the 2DEG at an AlGaAs/GaAs heterostructure. The three gates (to which voltages  $V_R$ ,  $V_L$ , and  $V_g$  are applied as indicated in the figure) at the lower arm are used for controlling the QD and the gate voltage  $V_C$  is for tuning the conductance of the upper arm. When the gate  $V_L$  is biased strongly, the system becomes a T-coupled QD as shown in Fig. 1 (b). The length of the QW, namely the distance between the QD and the junction at the lead, is about  $L \sim 1 \mu\text{m}$ .

In the addition spectrum of the QD, the discrete energy levels inside the QD are separated by the difference in the quantum confinement energy  $\Delta E$  and the single-electron charging energy  $E_C$ . We can shift the spectrum by the center gate voltage  $V_g$  to tune any one of them to the Fermi level. In the present sample, by measuring the conductance through the QD, we found that  $\Delta E$  and  $E_C$  are typically  $\sim 120 \mu\text{eV}$  and  $\sim 1 \text{ meV}$ , respectively. The gate on the upper arm  $V_C$  is used for tuning the conductance of this arm. We can make the device a T-coupled QD by applying a large negative voltage on  $V_L$  so that the transmission of electron underneath  $V_L$  is forbidden. This is topologically the same as the T-coupled QD shown in Fig. 1 (b). The distance between the QD and the junction at the lead is  $L \sim 1 \mu\text{m}$ . When required, we made this gate slightly transmissible in order to measure the AB signal through the system with the magnetic field ( $B$ ) applied perpendicular to the 2DEG.

Measurements were performed in a mixing chamber of a dilution refrigerator between 30 mK and 1 K by a standard lock-in technique in the two-terminal setup with an excitation voltage of  $10 \mu\text{V}$  (80 Hz, 5 fW) between the source and the drain. Noise filters were inserted into every lead below 1 K as well as at room temperature.

### III. RESULTS AND DISCUSSION

#### A. Emergence of the Fano Effect in the Conductance

We set  $V_L$  to  $-0.205 \text{ V}$  so as to forbid the electron transmission under it while  $V_R$  was  $-0.190 \text{ V}$  which made this gate slightly transmissible.  $V_C$  was adjusted to make the conductance of the system around  $2e^2/h$ , which is quasi-single channel condition. Figure 3 (a) shows typical results of the conductance through the system as a function of the gate voltage  $V_g$  at several temperatures ( $T$ ). Since the connecting QW between the lead QW and the QD is narrow and long, the QD would not affect the conduction through the lead QW in the classical transport regime. Correspondingly, at high temperatures above 800 mK, hardly any characteristic structure appears in the signal. Sharp dip structures, however, rapidly grow with lowering the temperature. They are anti-resonance (or reflection due to resonance) dips due to Coulomb oscillation in the QD. Furthermore, the resonant features are very asymmetric and varies widely in their lineshape. For example, at  $V_g = -0.485 \text{ V}$  and  $V_g = -0.47 \text{ V}$ , the lineshape consists of a sharp dip and an adjacent peak, while only asymmetric sharp dip structures appear between  $V_g = -0.45 \text{ V}$  and  $-0.38 \text{ V}$ .

These lineshapes in the conductance are characteristic of the Fano effect. Actually, the lineshape at the lowest temperature can be fitted to the following equation<sup>16,17</sup>

$$G_{\text{tot}} = A \frac{(\tilde{\epsilon} + q)^2}{\tilde{\epsilon}^2 + 1} + G_{\text{bg}}, \quad (1)$$

where  $G_{\text{bg}}$  is non-interfering contribution of the lead and is a smooth function of  $V_g$  that can be treated as a constant for each peak. The first term is the Fano contribution with an asymmetric parameter  $q$  where the normalized energy

$$\tilde{\epsilon} = \frac{\epsilon - \epsilon_0}{\Gamma/2} = \frac{\alpha(V_g - V_0)}{\Gamma/2}. \quad (2)$$

The parameters  $A$ ,  $\epsilon_0 \equiv \alpha V_0$ , and  $\Gamma$  represent the amplitude, the position, and the width of the Fano resonance, respectively.  $\alpha$  is the proportionality factor which relates  $V_g$  to the electro-chemical potential of the QD and given by  $\alpha = eC_g/C_{\text{tot}}$ , where  $C_g$  is the capacitance between the QD and the gate  $V_g$  and  $C_{\text{tot}}$  is the total capacitance. Note that the functional form of the Fano part in Eq. (1) can be applied to both resonance and anti-resonance. The parameters of the QD can be obtained from an independent measurement of the transport through the QD under an appropriate condition of the gate voltages (applying a large negative  $V_C$  to cut the upper conduction path and opening the lower path by decreasing  $V_L$ ). We estimate  $\alpha = 50 \pm 10 \mu\text{eV}/\text{mV}$  for the present system.

Figure 3 (b) shows typical results of the fitting for three dips. The satisfactory agreement assures that the Fano

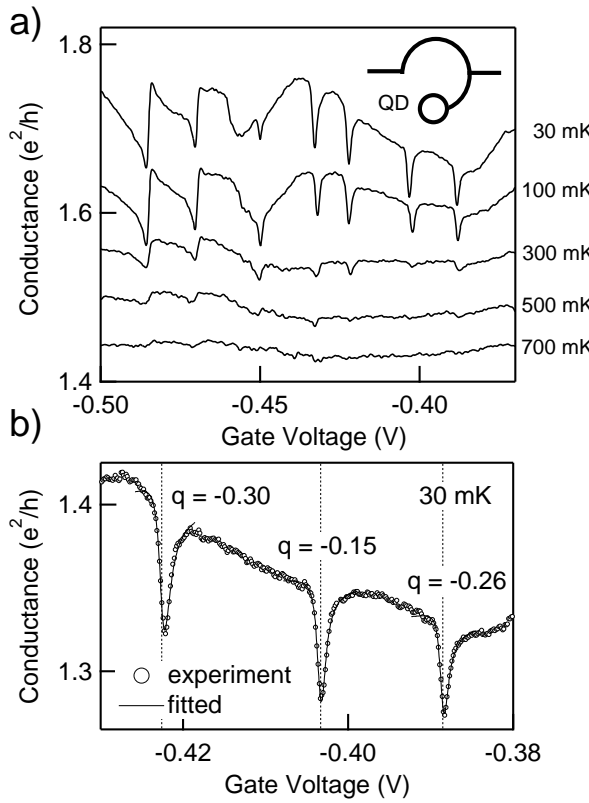


FIG. 3: (a) Conductance of the T-coupled QD as a function of  $V_g$  at several temperatures. As the temperature lowered, the Fano feature appeared. The magnetic field was 0.80 T. The curves for  $T < 700$  mK are incrementally shifted upwards for clarity. (b) Three Fano features in the conductance at 30 mK are fitted to Eq. (1). The obtained  $q$ 's are shown. The vertical dashed lines indicate the obtained discrete level position  $V_0$ 's.

state is formed in the T-coupled QD system. The obtained values of  $\Gamma$  are  $\sim 70$   $\mu$ eV, which is much larger than the thermal broadening  $3.5k_B T = 9$   $\mu$ eV at 30 mK (here,  $k_B$  is the Boltzmann constant). In Fig. 3 (b), the obtained  $q$ 's are also shown and the vertical dashed lines indicate the discrete level position ( $V_0$ ). Both the variation of  $q$  and that of the level spacing reflect that the conductance through this system reflects the characteristic of each of the single levels in the QD.

We note that the data in Fig. 3 (a) is obtained at  $B = 0.80$  T. The Fano effect in this system has been observed at several magnetic fields, as was also the case in the Fano effect in the QD-AB-ring system<sup>16,17</sup>. In the present case, the role of the magnetic field can be understood because the QW between the QD and the junction is curved as shown in Fig. 2, and the coupling is modified by the Lorentz force. In the previous reports<sup>16,17</sup> we have discussed that  $q$  should be a complex number in a QD-AB-ring geometry under finite  $B$ . This treatment is needed to describe the  $V_g$ - $B$  dependence of the lineshape to cover the wide range of  $B$ , when the interfering phase is modulated by  $B$ . For a fixed magnetic field, Eq. (1)

with a real  $q$  well describes the lineshape. Furthermore in the present case, since the effective area of the connecting QW is very small, the lineshape is found to be much less sensitive to the magnetic field than the case of an AB ring.

In the T-coupled geometry, the resonance is detected through the non-local conductance and the electric field of the modulation gate works only locally, and therefore it is easy to distinguish the coherent part from the incoherent part in the conductance. In contrast, the transmission experiments such as in the QD-AB-ring system usually gives the transmission probability including both the coherent and incoherent processes<sup>25</sup>. For example, in the case of Fano resonance in the AB geometry, ordinary Coulomb oscillation overlaps the coherent lineshape. In the case of simple AB magnetoresistance, the magnetic field is applied all over the specimen, and the AB oscillation is superposed on the background conductance fluctuation.

## B. Temperature Dependence of the Fano Effect

With increasing temperature, the dip structures is rapidly smeared out. The origins of such smearing due to finite temperature can be classified into thermal broadening and quantum decoherence. The former should be taken into account when  $3.5k_B T$  becomes the same order of magnitude as  $\Gamma$  at  $T = 200$  mK. Henceforth we concentrate ourselves on the thermal broadening and examine whether it alone can explain the observed diminishment of the resonance structure.

The thermal broadening appears in the distribution in  $\tilde{\epsilon}$  in the Fano transmission form Eq. (1). As noted in the previous paper<sup>17</sup>, the formula Eq. (1) is derived assuming point-interaction between the localized states and the continuum. However in the present system, the length of the connecting QW is finite and dephasing during the traversal due to thermal broadening may be important. If such dephasing can be ignored,  $q$  can be treated as a real number as noted above. Conversely, the dephasing inside the connecting QW requires to use complex  $q$ 's<sup>19</sup>.

In order to treat the thermal broadening quantitatively, we model a simple quantum circuit for the present system as shown in Fig. 4 (a). The QD is simply expressed as a tunable resonator consisting of a tunnel barrier and a perfect reflector. The phase shift of the reflector is approximated to be proportional to the gate voltage around the resonance. The connecting QW between the QD and the T-junction is simply a phase shifter of  $kL$  ( $k$  : wave vector). We put the S-matrix for the junction  $S_T$  as

$$\begin{pmatrix} b_1 \\ b_2 \\ b_3 \end{pmatrix} = S_T \begin{pmatrix} a_1 \\ a_2 \\ a_3 \end{pmatrix}, \quad S_T = \begin{pmatrix} \frac{1-a}{2} & -\frac{1+a}{2} & \sqrt{\frac{1-a^2}{2}} \\ -\frac{1+a}{2} & \frac{1-a}{2} & \sqrt{\frac{1-a^2}{2}} \\ \sqrt{\frac{1-a^2}{2}} & \sqrt{\frac{1-a^2}{2}} & a \end{pmatrix}, \quad (3)$$

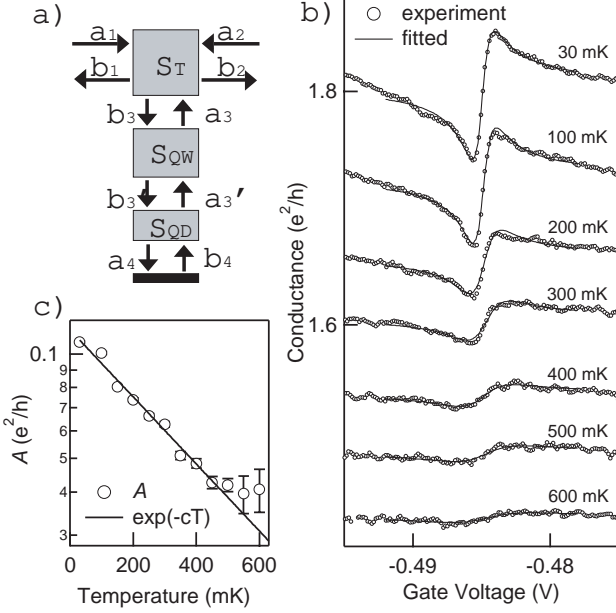


FIG. 4: (a) Model of the quantum circuit that consists of the T-junction, the QW and the QD. Also see Fig. 1 (a). (b) Experimental data (open circles) and the fitted curves. The data for  $T < 600$  mK are incrementally shifted upwards for clarity. (c) Obtained  $A$  value as a function of temperature. The solid line shows the exponential decay  $\propto \exp(-cT)$  with  $c = 2.0 \text{ K}^{-1}$ .

to keep the unitarity<sup>26</sup>.  $\{a_i\}$  and  $\{b_i\}$  are amplitudes of incoming and outgoing waves, as shown in Fig. 4 (a). Here we take  $a$  as a real number, which determines the direct reflection coefficient at the junction. The S-matrix for the QW (phase shifter) is expressed as

$$\begin{pmatrix} a_3 \\ b'_3 \end{pmatrix} = S_{QW} \begin{pmatrix} b_3 \\ a'_3 \end{pmatrix}, \quad S_{QW} = \begin{pmatrix} 0 & e^{i\beta} \\ e^{i\beta} & 0 \end{pmatrix}, \quad \beta \equiv kL. \quad (4)$$

And the S-matrix for the tunnel barrier can be written as

$$\begin{pmatrix} a'_3 \\ a_4 \end{pmatrix} = S_{QD} \begin{pmatrix} b'_3 \\ b_4 \end{pmatrix}, \quad S_{QD} = \begin{pmatrix} \cos\phi & i\sin\phi \\ i\sin\phi & \cos\phi \end{pmatrix}. \quad (5)$$

Lastly the reflector with a variable phase shift of  $\theta$  is simply expressed as

$$b_4 = e^{i\theta} a_4. \quad (6)$$

By calculating the combined S-matrix, the complex transmission coefficient of the system is obtained as

$$t = \frac{1+a}{2} \cdot \frac{-1 - e^{i(\theta+2\beta)} + (e^{2i\beta} + e^{i\theta}) \cos\phi}{1 + ae^{i(\theta+2\beta)} - (ae^{2i\beta} + e^{i\theta}) \cos\phi}, \quad (7)$$

where

$$\beta = kL = k_F L + \frac{L}{\hbar v_F} (\epsilon - \mu). \quad (8)$$

Here,  $\mu$  is the position of the chemical potential.  $L$ ,  $k_F$ , and the Fermi velocity  $v_F$  are estimated from the experimental conditions. The resonance of the QD occurs at  $\theta = 0$  hence  $\theta$  is taken as  $b(\epsilon - \mu)$ . It is easy to see  $|t|^2$  numerically reproduces Eq. (1) near the resonance.

The conductance of the system at the low bias ( $\ll kT$ ) can be expressed by the Landauer-Büttiker formula as<sup>18</sup>

$$G_{tot} = A \int d\epsilon |t|^2 \frac{1}{4kT} \cosh^{-2} \left( \frac{\epsilon - \mu}{2kT} \right) + G_{bg}. \quad (9)$$

We treat  $a$ ,  $b$ ,  $V_0$ , and  $G_{bg}$  as fitting parameters. While  $V_0$  and  $G_{bg}$  are slightly dependent on temperature due to the neighboring Fano resonances,  $a$  and  $b$  are treated as temperature independent.  $A$  is left temperature-dependent to absorb decoherence other than thermal broadening.

We found that the fitting is insensitive to the value of  $a$  as long as it is smaller than  $\sim 0.3$ , which suggests that the specific form of  $S_T$  in Eq. (3) does not affect the generality. Figure 4 (b) shows the results of the successful fitting for  $a = 0$ . Note that the number of the crucial fitting parameters is very small since most of the parameters can be determined at the lowest temperature and taken as temperature independent. Amplitude  $A$  is shown in Fig. 4 (c) as a function of temperature. At 600 mK, the amplitude  $A$  still remains  $\sim 40\%$  of that at the lowest temperature. The observed strong temperature dependence, therefore, is mostly due to the thermal broadening in the QW. If we set  $L$  to zero, the temperature dependence of Eq. (9) would be much weakened.

Interestingly, the behavior of  $A$  is well fitted to  $\propto \exp(-cT)$  with  $c = 2.0 \text{ K}^{-1}$  between 30 mK and 500 mK. Such temperature dependence of the coherence is reminiscent of that in an AB ring with the local and non-local configurations<sup>27</sup>, where the temperature dependence of the AB amplitude was found to be weaker in the non-local setup than in the local setup. Theoretically it was pointed out that the difference in the impedance of the probes seen from the sample is important<sup>28</sup>. In the present case, since one end of the QD is cut and non-local effect is observed, the impedance seen from the sample (namely, the QD and the QW connecting it to the lead) is very high and the situation is basically the non-local one they treated. Hence the discussion in Ref. [28] might be applicable here. In the present case, however, we do not have the data that corresponds to the “local” setup and can be compared with the present ones.

### C. Phase Measurement of Electrons at a QD

Next, we discuss application of the present geometry for measurement of the phase evolution at the QD. While the QD-AB-ring geometry has been used for this purpose<sup>4,5,6,7,8,9</sup>, the T-coupled QD should also provide information on the phase shift by the QD. Since in Eq. (7), the dip structure is mainly due to the resonance and

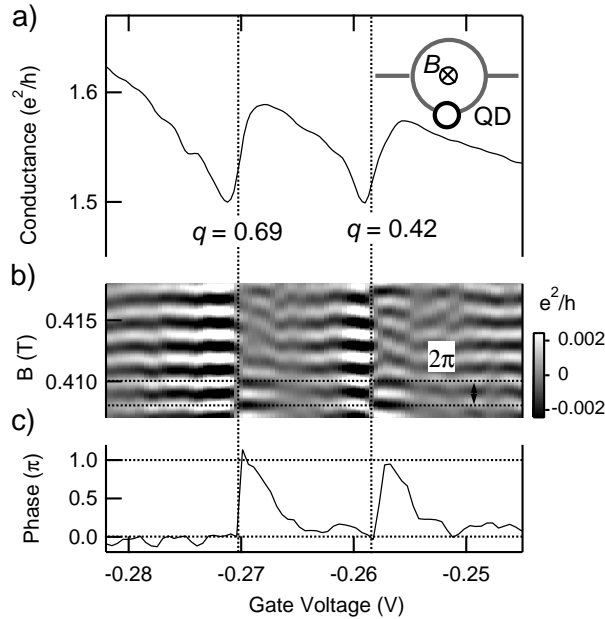


FIG. 5: (a) Two resonance dips in the conductance as a function of  $V_g$  at 30 mK at  $B = 0.405$  T. The system now allows electrons to transmit through the QD. The vertical lines indicate the positions of the discrete energy levels in the QD. Note that the  $q$  values are positive. (b) Gray-scale plots of the AB oscillation component of the system as a function of  $V_g$  and  $B$ . (c) Phase of the AB oscillation obtained at each  $V_g$ .

phase shift in the QD, we can, in principle, extract information on the phase shift. If we restrict ourselves around the resonance point, we can utilize the simple Fano formula [Eq. (1)], instead of the complicated analysis by using the quantum circuit in the previous section. To see this, we made the gate  $V_L$  slightly open and allowed electrons to pass the QD. The system is now a QD-AB-ring system rather than a T-coupled QD and the Fano effect in both the reflection mode and the transmission mode is expected to occur.

Figure 5 (a) shows the conductance of the system as a function of  $V_g$ , where two resonance dips showing Fano lineshape are plotted. The dashed lines indicate the positions of the discrete energy levels in the QD that are obtained by the aforementioned fitting procedure. The values of the asymmetric parameter  $q$  are given in the figure. Note that the direction of the asymmetric tail, namely the sign of  $q$ , are the same for both dips.

Because the conduction through the lower arm is kept very low, these Fano features change little by the slight variation of  $B$ , although there exists coherent component in the transmission through the QD, which appears as a small oscillation in conductance versus  $B$ . This is the AB oscillation whose period is 2.0 mT as expected from the ring size. The AB oscillation was measured at each  $V_g$  and the AB component was extracted by fast Fourier transformation (FFT). Figure 5 (b) shows the obtained

AB component in the gray-scale plot as a function of  $V_g$  and  $B$ . The coherent component through the QD is only of the order of  $\sim 0.005e^2/h$ , in clear contrast with the net signal up to the order of  $\sim 0.08e^2/h$  [Fig. 5 (a)].

Now, we focus on the behavior of the phase of the AB oscillation. We traced the conductance maximum as a function of  $V_g$  and plotted in Fig. 5 (c) in the unit of the AB period. The phase abruptly changes by  $\pi$  just at the resonance points. Such phase lapse that occurs in the energy scale much smaller than  $\Gamma$ , reflects the two-terminal nature of the present QD-AB-ring system. The AB oscillations at both dips are in-phase. This is consistent with the previous report<sup>4</sup>. Although the origin of the in-phase nature of the Coulomb peak is still under debate in spite of several theoretical works<sup>10,29,30,31,32,33,34</sup>, it is clear that the sign of  $q$  is the same for both dips reflecting the in-phase nature. This result, which reproduces for other peaks in the present experiment, demonstrates that “phase measurement” can be performed simply by observing the sign of  $q$ , without investigating the AB oscillation. Interestingly, there also exists another slow  $\pi$  phase shift away from the resonance point commonly for these peaks, leading to the in-phase nature of them. Such behavior is consistent with what we observed in the Fano effect in the transmission mode<sup>16,17</sup>.

#### IV. CONCLUSION

In conclusion, we have realized the Fano effect in a QW with a side-coupled QD. The temperature dependence of the resonance structure was analyzed by including the thermal broadening, which turned out to be mostly responsible for the rapid smearing of the resonances. We have shown that the phase measurement of electrons at a QD is also possible in this geometry and gives a consistent result with that by a QD-AB-ring system. While such a simple geometry as the T-coupled QD has never been investigated experimentally, its clear advantage lies in that only coherent signal associated with the QD is obtained. This work proves that the Fano effect in this interferometer can be the powerful tool to measure the coherence and the phase of electrons.

#### ACKNOWLEDGMENTS

We thank F. B. Anders, M. Eto, T. Ihn, J. König, and A. Schiller for helpful comments. This work is supported by a Grant-in-Aid for Scientific Research and by a Grant-in-Aid for COE Research (“Quantum Dot and Its Application”) from the Ministry of Education, Culture, Sports, Science, and Technology of Japan. K.K. is supported by a Grant-in-Aid for Young Scientists (B) (No. 14740186) from Japan Society for the Promotion of Science.

---

<sup>1</sup> R. A. Webb, S. Washburn, C. P. Umbach, and R. B. Lai-bowitz, Phys. Rev. Lett. **54**, 2696(1985).

<sup>2</sup> C. G. Smith, M. Pepper, H. Ahmed, J. E. F. Frost, D. G. Hasko, R. Newbury, D. C. Peacock, D. A. Ritchie and G. A. C. Jones, J. Phys.:Condensed Matter **1**, 9035 (1989).

<sup>3</sup> Y. Ji, Y. Chung, D. Sprinzak, M. Heiblum, D. Mahalu, and H. Shtrikman, Nature **422**, 415 (2003).

<sup>4</sup> A. Yacoby, M. Heiblum, D. Mahalu, and H. Shtrikman, Phys. Rev. Lett. **74**, 4047 (1995).

<sup>5</sup> S. Katsumoto and A. Endo, J. Phys. Soc. Jpn. **65**, 4086 (1996).

<sup>6</sup> R. Schuster, E. Buks, M. Heiblum, D. Mahalu, V. Uman-sky, and H. Shtrikman, Nature **385**, 417 (1997).

<sup>7</sup> W. G. van der Wiel, S. De Franceschi, T. Fujisawa, J. M. Elzerman, S. Tarucha, and L. P. Kouwenhoven, Science **289**, 2105 (2000).

<sup>8</sup> Y. Ji, M. Heiblum, D. Sprinzak, D. Mahalu, and H. Shtrik-man, Science **290**, 779 (2000).

<sup>9</sup> Y. Ji, M. Heiblum, and H. Shtrikman, Phys. Rev. Lett. **88**, 076601 (2002).

<sup>10</sup> A. L. Yeyati and M. Büttiker, Phys. Rev. B **52**, 14360 (1995).

<sup>11</sup> U. Fano, Phys. Rev. **124**, 1866 (1961).

<sup>12</sup> For example, U. Fano and A. R. P. Rau, *Atomic Collisions and Spectra* (Academic Press, Orland , 1986); F. Cerdeira, T. A. Fjeldly, and M. Cardona, Phys. Rev. B **8**, 4734 (1973); J. Faist, F. Capasso, C. Sirtori, K. W. West, and L. N. Pfeiffer, Nature **390**, 589 (1997).

<sup>13</sup> E. Tekman and P. F. Bagwell, Phys. Rev. B **48**, 2553 (1993).

<sup>14</sup> J. U. Nöckel and A. D. Stone, Phys. Rev. B **50**, 17415 (1994).

<sup>15</sup> P. Singha Deo and A. M. Jayannavar, Mod. Phys. Lett. B **10**, 787 (1996); P. Singha Deo Solid St. Commun. **107**, 69 (1998); C.-M. Ryu and S. Y. Cho, Phys. Rev. B **58**, 3572 (1998); K. Kang, Phys. Rev. B **59**, 4608 (1999); O. Entin-Wohlman, A. Aharonov, A., Y. Imry, and Y. Levin-son, J. Low Temp. Phys. **126**, 1251 (2002); W. Hofstetter, J. König, and H. Schoeller, Phys. Rev. Lett. **87**, 156803 (2001); Tae-Suk Kim, Sam Young Cho, Chul Koo Kim, and Chang-Mo Ryu: Phys. Rev. B **65**, 245307 (2002).

<sup>16</sup> K. Kobayashi, H. Aikawa, S. Katsumoto, and Y. Iye, Phys. Rev. Lett. **88**, 256806 (2002).

<sup>17</sup> K. Kobayashi, H. Aikawa, S. Katsumoto, and Y. Iye, to appear in Phys. Rev. B.

<sup>18</sup> Kicheon Kang, Sam Young Cho, Ju-Jin Kim, and Sung-Chul Shin, Phys. Rev. B **63**, 113304 (2001).

<sup>19</sup> A. A. Clerk, X. Waintal, and P. W. Brouwer Phys. Rev. Lett. **86**, 4636 (2001).

<sup>20</sup> Maria A. Davidovich, E. V. Anda, C. A. Busser, and G. Chiappe, Phys. Rev. B **65**, 233310 (2002).

<sup>21</sup> A. A. Aligia and C. R. Proetto, Phys. Rev. B **65**, 165305 (2002).

<sup>22</sup> M. E. Torio, K. Hallberg, A. H. Ceccatto, and C. R. Proetto, Phys. Rev. B **65**, 085302 (2002).

<sup>23</sup> R. Franco, M. S. Figueira, E. V. Anda Phys. Rev. B **67**, 155301 (2003).

<sup>24</sup> R. M. Konik, cond-mat/0207622 (2002).

<sup>25</sup> For example, H. Aikawa, K. Kobayashi, A. Sano, S. Katsumoto, and Y. Iye, cond-mat/0309084 (2003).

<sup>26</sup> M. Büttiker, Y. Imry, and M. Ya. Azbel, Phys. Rev. A **30**, 1982 (1984); Björn Kubala and Jürgen König, Phys. Rev. B **67**, 205303 (2003).

<sup>27</sup> K. Kobayashi, H. Aikawa, S. Katsumoto, and Y. Iye, J. Phys. Soc. Jpn. **71**, L2094 (2002).

<sup>28</sup> G. Seelig, S. Pilgram, A. N. Jordan, and M. Büttiker, Phys. Rev. B **68**, R161310 (2003); see also G. Seelig and M. Büttiker, Phys. Rev. B **64**, 245313 (2001).

<sup>29</sup> C. Bruder, R. Fazio, and H. Schoeller, Phys. Rev. Lett. **76**, 114 (1996).

<sup>30</sup> Y. Oreg and Y. Gefen, Phys. Rev. B **55**, 13726 (1997).

<sup>31</sup> J. Wu, B.-L. Gu, H. Chen, W. Duan, and Y. Kawazoe, Phys. Rev. Lett. **80**, 1952 (1998).

<sup>32</sup> G. Hackenbroich and H. Weidenmüller, Europhys. Lett. **38**, 129 (1997).

<sup>33</sup> H.-W. Lee, Phys. Rev. Lett. **82**, 2358 (1999).

<sup>34</sup> T. Taniguchi and M. Büttiker, Phys. Rev. B **60**, 13814 (1999).